Why Sliding Friction of Ne and Kr Monolayers Is So Different on the Pb(111) Surface

Y. N. Zhang,[1] F. Hanke,[2] V. Bortolani,[3] M. Persson,[2,4] and R. Q. Wu[1]

[1]*Department of Physics and Astronomy, University of California, Irvine, California, 92697 USA*
[2]*The Surface Science Research Center, The University of Liverpool, Liverpool, L69 3BX, United Kingdom*
[3]*Dipartimento di Fisica e CNISM, Università di Modena e Reggio Emilia, Via Campi 213/A, Modena, 41100 Italy*
[4]*Department of Applied Physics, Chalmers University of Technology, SE-412 96, Göteborg, Sweden*

(Received 14 December 2010; revised manuscript received 11 May 2011; published 8 June 2011)

To understand the tribological properties of Ne and Kr on Pb(111), the potential energy surfaces for sliding motion of Ne, Kr, and Xe monolayers on the Pb(111) surface are examined through density functional calculations, using either local density or self-consistent nonlocal van der Waals functionals. The calculated adsorption energy for Xe/Pb(111) agrees well with experiment, validating the present approach and parameters. Activation energies along a sliding path indicate that Ne motion is much faster than Kr and Xe on Pb(111) at $T \sim 6$ K, which explains the puzzling experimental observation.

DOI: 10.1103/PhysRevLett.106.236103 PACS numbers: 68.35.Af, 68.43.Bc, 71.15.Nc

The continuing advances in surface physics make it now possible to study tribological properties of various materials at the atomic scale and to reach an unprecedented level of understanding on the origin of friction [1]. Recent measurements performed with apparatuses such as quartz crystal microbalance (QCM) [2,3] and atomic force microscopy [4,5] established that the friction laws at the nanoscale are different from the macroscopic Amontons laws. Intriguing and sometimes puzzling experimental observations have stimulated new theoretical studies of friction, aiming at the development of clear microscopic understandings on friction and wear. The difficulties in testing hypotheses are known to be a major theoretical problem. While a tremendous number of parameters may affect the theoretical results of lateral forces between two solids, macroscopic measurements only provide a single number: the friction coefficient. This situation made the validation or falsification of theories practically impossible. The advent of controlled atomic scale measurements substantially changed the situation and new computational techniques on the other hand enable theorists to study models that include the relevant internal degrees of freedom of the contacting surfaces. Indeed, theoretical studies [6–10] of friction have touched on various effects such as electron-hole pair excitations, chemical reactions, vibration relaxations, and the dynamics of defect creation and diffusion.

Because of the weak interaction across interfaces, systems with adsorption of rare-gas (RG) atoms on solid surfaces are ideal to tackle tribological issues at the atomic level. The Pb(111) surface was frequently used as a substrate since it is possible to deposit several layers of Pb on the quartz electrode in UHV for the convenience of QCM measurements. Furthermore, surface morphologies measured with scanning tunneling microscopy indicate the presence of wide atomic terraces with a size of about 50 nm on Pb(111) [11], much larger than the typical QCM oscillating amplitude of ~5 nm. One striking finding in this context is the drastic difference between the sliding friction of Ne and Kr mono- or multilayers [12]. While it was shown that one or a few monolayers of Ne slide on Pb (111) and a slip time is measurable (~3 nanoseconds), Kr layers are pinned (slip time is essentially zero) at low temperature (~6.5 K). The present study is devoted to the microscopic explanation of this unusual behavior. We have calculated the potential energy surfaces for Ne, Kr and Xe monolayers on Pb(111). Indeed, the Pb(111) surface is found to be substantially ''rougher'' for Kr than for Ne, as manifested by significantly different activation energies for their sliding motion, in good agreement with experimental observations.

To simulate RG/Pb(111), we used a periodic model with a seven-layer slab for Pb(111), a monolayer of RG adatoms, and a ~20 Å thick vacuum region. As depicted in Fig. 1(a), a $(\sqrt{3} \times \sqrt{3})R30°$ supercell was adopted. This cell is the simplest commensurate structure for RG monolayers on close-packed metal surfaces, as revealed by LEED measurements [13,14], and also as used in previous theoretical studies [15]. Density functional theory calculations were performed using the Vienna *ab initio* simulation package (VASP) [16] along with projector augmented wave pseudopotentials [17]. An $(8 \times 8 \times 1)$ Monkhorst-Pack k-point grid was used to sample the Brillouin zone and an energy cutoff of 400 eV was used for the basis expansion. We fully optimized positions of adatoms and the top five Pb layers and fixed the two bottommost Pb layers at their bulk positions.

Recent *ab initio* calculations indicated that the local-density approximation (LDA) and generalized-gradient approximation [18] gave inconsistent descriptions for the structural properties of RG adsorption on metal surfaces, and LDA was found to yield better results [19,20]. Nevertheless, one needs to be cautious in dealing with sliding problems of RG since the energetics might be

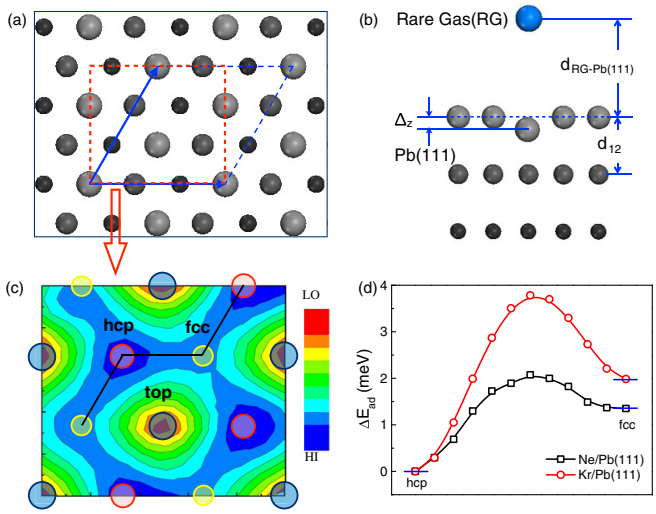

FIG. 1 (color online). Panels (a) and (b) are top and side views of the atomic model adopted in the present calculations. The parallelogram and rectangle in (a) show the $\sqrt{3} \times \sqrt{3}$ unit cell, and the "mapping" region displayed in panel (c), respectively. The large, medium, and small spheres are for the surface, subsurface, and third layer Pb atoms and notations $d_{RG\text{-}Pb(111)}$ and Δ_z are marked in for the convenience of discussions. Panels (c) and (d) show results for Ne/Pb(111) using LDA: contours of E_{ad} and changes of E_{ad} along the path hcp → bridge → fcc, respectively.

affected by the van der Waals (vdW) interactions that are missing in traditional density functional calculations [21–23]. In the present studies, we first treated the exchange-correlation effect at the level of LDA and, furthermore, investigated the influence of vdW interactions using the nonlocal energy functional (vdW-DF) proposed by Langreth and Lundqvist [24] as implemented self-consistently in VASP by Klimeš, Bowler, and Michaelides [25]. As an exchange term, we used the OPTB86B version [25], which gives a lattice constant of 4.98 Å for the bulk Pb, in close agreement with experiments, when including the 5*d* shell of Pb as valence electrons in the projector augmented wave. As a benchmark for the studies of energetics, the calculated adsorption energy [defined as $E_{ad} = E_{tot} - E_{Pb(111)} - E_{RG\text{-}ML}$ where E_{tot}, $E_{Pb(111)}$, and $E_{RG\text{-}ML}$ are total energies of RG/Pb(111), Pb(111), and the isolated RG monolayer, respectively] of Xe/Pb(111) is 172.6 meV, close to the experimental value, 191 ± 10 meV [26].

Although friction depends on the effective dissipation of kinetic energies of atoms, the simplest picture would connect the sliding friction to the hopping probability of adatoms between adjacent stable and metastable sites. To quantitatively describe the "roughness" of Pb(111) toward the sliding motion of RG adatoms, we sampled the $\sqrt{3} \times \sqrt{3}$ supercell with about 40 mesh points in the real space, and calculated the position dependence of E_{ad}. These data were used to construct potential energy surfaces, as displayed in Fig. 1(c) for Ne/Pb(111) from the LDA calculations. According to results for high-symmetric geometries in Table I, both Ne and Kr prefer the high-coordination hcp-hollow site, and disfavor the low-coordination atop site. The energy differences between the atop and hcp adsorption geometries within LDA are 7.8 meV and 14.9 meV for Ne/Pb(111) and Kr/Pb(111), respectively. The corresponding values obtained within the vdW-DF are somewhat smaller: 4.8 and 9.8 meV for Ne and Kr on Pb(111).

TABLE I. The adsorption energy, E_{ad} (meV), and interlayer distance, $d_{RG\text{-}Pb(111)}$ (Å), for symmetric structures of Ne/Pb(111) and Kr/Pb(111), obtained through LDA and vdW-DF (OPTB86B exchange) calculations. The activation energy, E_a (meV), is also given for RG sliding motion.

	Ne		Kr	
	LDA	vdW-DF	LDA	vdW-DF
E_{ad}^{atop}	−36.3	−46.8	−82.1	−125.1
E_{ad}^{fcc}	−42.7	−51.3	−95.0	−133.9
E_{ad}^{hcp}	−44.1	−51.6	−97.0	−134.9
$d_{RG\text{-}Pb(111)}^{atop}$	3.3	3.8	3.7	3.9
$d_{RG\text{-}Pb(111)}^{hcp,fcc}$	3.0	3.5	3.5	3.8
E_a	2.1	0.7	3.8	2.5

It is significant to note in Table I that the inclusion of vdW interactions does not alter the site preference for Ne and Kr, despite the noticeable changes of bond lengths and adsorption energies. To better appreciate this result, LDA and vdW-DF adsorption energies are plotted in Fig. 2 against the interplanar distance for Ne over the high-symmetric sites of Pb(111). While the potential wells are deepened in vdW-DF compared to LDA, Ne and Kr both still favor the hcp site. Meanwhile, the distances,

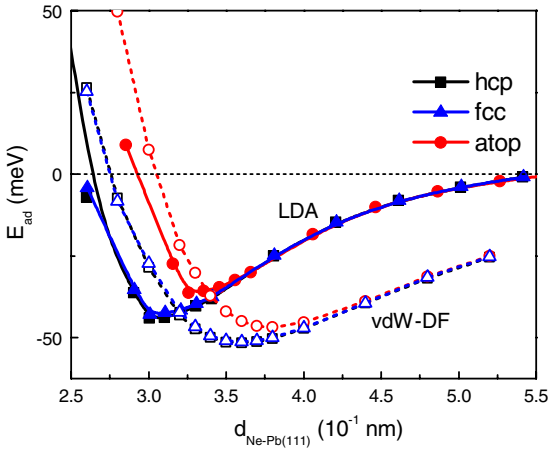

FIG. 2 (color online). The position and distance dependent adsorption energies of Ne/Pb(111). Solid and open symbols represent results from the LDA and vdW-DF using the OPTB86B exchange term, respectively.

$d_{\text{RG-Pb(111)}}$, expand by ~0.2–0.5 Å from the LDA data. The induced relaxations on Pb(111), Δ_z in Fig. 1(b), are smaller than 0.01 Å.

The contours of E_{ad} in Fig. 1(c) show that RG atoms slide on Pb(111) along a "zigzag" route as highlighted by the lines, hcp → bridge → fcc → bridge → hcp, under the influence of lateral pushing forces. To appreciate the difference between Ne and Kr, we present their results of $\Delta E_{\text{ad}} = E_{\text{ad}}^{\text{site}} - E_{\text{ad}}^{\text{hcp}}$ along the path hcp → bridge → fcc in Fig. 1(d). The activation energies, E_a, can be directly calculated from the change of E_{ad} between the ground state and transition state, which occurs over the bridge site for both Ne and Kr adatoms. It is striking to see that values of E_a are very different: 2.1 (0.7) meV for Ne versus 3.8 (2.5) meV for Kr through LDA (vdW-DF) calculations. Using the Arrhenius equation with $E_{a,\text{Kr}} - E_{a,\text{Ne}} =$ 1.7 meV (LDA) or 1.8 meV (vdW-DF) and $T = 6.5$ K, one can estimate that Kr hopping should be more than 20 times slower than Ne, even without considering the mass effect of Kr on the frequency factor. Obviously, the "unusual" difference between the sliding friction properties observed for Ne and Kr on Pb(111) mainly stems from the difference between their E_a [12].

Now one may ask: "What makes the values of E_a different for Ne and Kr?" An important quantity for the understanding of the bonding mechanism is the electron density difference, $n(\boldsymbol{r}) = n_{\text{RG/Pb(111)}}(\boldsymbol{r}) - n_{\text{Pb(111)}}(\boldsymbol{r}) - n_{\text{RG-ML}}(\boldsymbol{r})$, obtained from electron densities of RG/Pb(111), Pb(111), and the isolated RG monolayer, respectively. Plots of $\Delta n(\boldsymbol{r})$ for Ne/Pb(111) and Kr/Pb(111) in Fig. 3 show that electrons of RG adatoms obviously polarize toward the substrate, in consistence with previous studies of RG adsorptions on metal surfaces [20]. The contrasts between Ne and Kr manifest themselves through (1) the magnitude of $\Delta n(\boldsymbol{r})$ of Ne/Pb(111) being notably weaker than that of Kr/Pb(111), (2) the influence of Kr extending to interior Pb layers, whereas Ne appears to only affect the top Pb layer. It is more clear from the $\Delta n(z)$ curves in the middle panel in Fig. 3, the planar averages of $\Delta n(\boldsymbol{r})$ along the vertical direction, that the amplitude of electron polarization in Kr/Pb(111) is about 2 times larger than that in Ne/Pb(111). The disturbance of Ne fades quickly below the surface Pb layer, in contrast to the oscillating $\Delta n(z)$ of Kr in this region. While the stronger charge polarization of Kr leads to larger E_{ad}, the range of disturbance is crucial for the distinction between Kr and Ne in their E_a as well as ΔE_{ad} between the fcc and hcp sites.

More information can be unraveled from the partial density of states (PDOS) in Fig. 4. One may easily see a major dissimilarity between Ne and Kr: the p states of Ne are located at −9.7 eV whereas those of Kr are located at −5.6 eV. As shown by the shaded regions in Fig. 4(a), Pb has a large band gap between its s and p states above −6.5 eV. Ne p states overlap with Pb s states in energy and they have a weak hybridization in the energy range between −10.2 eV and −8.2 eV. The Kr p states, on the other hand, are located right in the Pb band gap and thus the Kr-Pb hybridization is weak. The topmost Pb atoms are slightly affected by RG adatoms, as demonstrated by curves of ΔDOS in Fig. 4(b) ($\Delta\text{DOS} = \text{DOS}_{\text{Pb in RG/Pb(111)}} - \text{DOS}_{\text{Pb in Pb(111)}}$). Some Pb s states

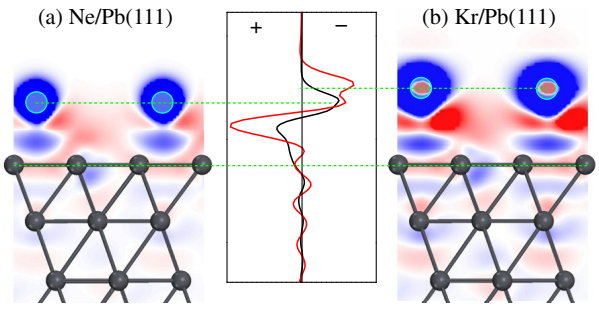

FIG. 3 (color online). Electron density differences of (a) Ne and (b) Kr on Pb(111) shown in the $(11\bar{2})$ plane within the range of $\pm 8 \times 10^{-5} e/\text{Å}^3$. Red (light gray) and blue (dark gray) represent electron accumulation and depletion, respectively. Line profiles in the middle show the planar averages of $\Delta n(\mathbf{r})$ along the surface normal, with the black line for Ne/Pb(111) and red (gray) line for Kr/Pb(111).

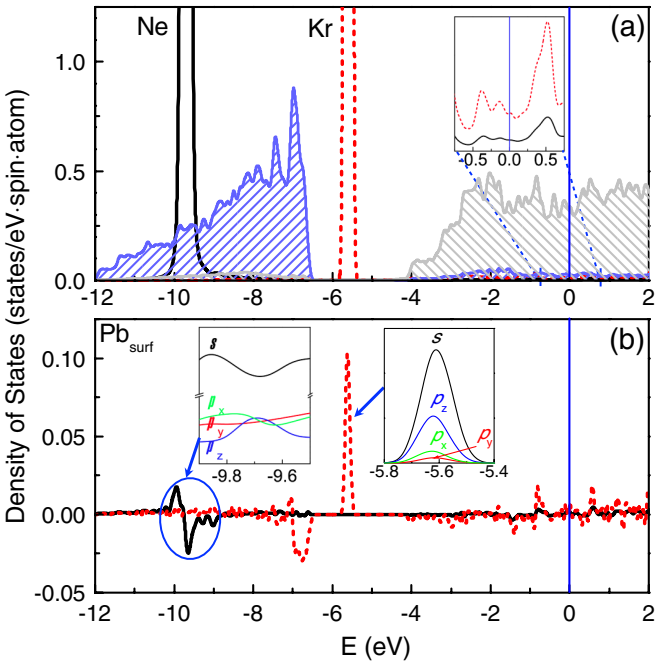

FIG. 4 (color online). (a) PDOS around Ne (solid line) and Kr (dashed line) on Pb(111); the inset displays the induced p states of Ne and Kr around the E_F; the blue (dark gray) and light gray shaded regions give the s and p states of around the Pb atoms. (b) The RG-induced change in PDOS of the topmost Pb atom; the insets show contributions from different s and p partial waves around the Pb surface atom at −9.7 eV in Ne/Pb(111) and at −5.6 eV in Kr/Pb(111), respectively. The vertical lines indicate the position of the Fermi level.

shift down in energy around −9.7 eV, a signature of Ne-Pb hybridization in Ne/Pb(111). In the left-side inset of Fig. 4(b), one finds energy splittings between p_z and $p_{x,y}$ states of Ne, due to the crystal field effect from the substrate. Strikingly, Kr produces a pronounced peak at −5.6 eV in the ΔDOS curve of Pb_{surf} in Fig. 4(b), as well as in the second and third Pb layers (not shown here). Further decomposition of this peak reveals its s and p_z contributions, as shown in the right-side inset of Fig. 4(b). It is clear from these DOS curves that RG-Pb interactions mainly occur in the low-energy region. Both DOS and ΔDOS of Ne and Kr are very small around the Fermi level in Figs. 4(a) and 4(b). Therefore, changes of Pb properties around E_F (e.g., going through superconducting transition) affect the friction negligibly [27].

In summary, we performed LDA and self-consistent vdW-DF calculations to explain the unusual difference between the observed sliding friction of Ne and Kr monolayers on the Pb(111) surface. Ne and Kr prefer the hcp-hollow site in their equilibrium adsorption geometries and slide along a path over hcp → bridge → fcc → bridge → hcp sites. However, the activation energy of Ne is noticeably smaller than that of Kr, which leads to a huge difference between their mobilities on Pb(111) at 6.5 K. Analyses of electronic properties reveal substantial charge polarization from RG adatoms toward the substrate as well as orbital intermixing in the interfacial region. In particular, the long-range disturbance of Kr in Pb is identified as the key factor for the pinning of Kr on Pb(111) at low temperature. As a prediction, the calculated E_a for the Xe monolayer sliding on Pb(111) is also large, 4.1 meV with the LDA, and the Xe monolayer also should be pinned by the substrate at low temperature. The present work provides a valuable example of using density functional simulations for quantitative studies of friction at the nanoscale, via the direct determination of potential energy surfaces and activation energies.

This work was supported by the DOE-BES (Grant No. DE-FG02-05ER46237). Calculations were performed on parallel computers at NERSC and those provided by SNAC and VR in Sweden.

[1] B. N. J. Persson, *Sliding Friction: Physical Principles and Applications* (Springer, Berlin, 1998).
[2] J. Krim and A. Widom, Phys. Rev. B **38**, 12 184 (1988).
[3] J. Krim, D. H. Solina, and R. Chiarello, Phys. Rev. Lett. **66**, 181 (1991).
[4] G. Binnig, C. F. Quate, and C. Gerber, Phys. Rev. Lett. **56**, 930 (1986).
[5] C. M. Mate, G. M. McClelland, R. Erlandsson, and S. Chiang, Phys. Rev. Lett. **59**, 1942 (1987).
[6] B. N. J. Persson, Phys. Rev. B **48**, 18 140 (1993).
[7] A. Franchini, M. Brigazzi, G. Santoro, and V. Bortolani, J. Phys. Condens. Matter **19**, 305 014 (2007); **20**, 224 019 (2008).
[8] Y. Mo, K. T. Turner, and I. Szlufarska, Nature (London) **457**, 1116 (2009).
[9] V. Bortolani, A. Franchini, G. Santoro, and M. Brigazzi, Tribol. Lett. **39**, 251 (2010).
[10] M. Persson, Solid State Commun. **80**, 917 (1991).
[11] L. Bruschi, G. Fois, A. Pontarollo, G. Mistura, B. Torre, F. Buatier de Mongeot, C. Boragno, R. Buzio, and U. Valbusa, Phys. Rev. Lett. **96**, 216101 (2006).
[12] L. Bruschi, M. Pierno, G. Fois, F. Ancilotto, G. Mistura, C. Boragno, F. Buatier de Mongeot, and U. Valbusa, Phys. Rev. B **81**, 115419 (2010).
[13] M. Caragiu, Th. Seyller, and R. D. Diehl, Phys. Rev. B **66**, 195411 (2002).
[14] C. Hückstädt, S. Schmidt, S. Hüfner, F. Forster, F. Reinert, and M. Springborg, Phys. Rev. B **73**, 075409 (2006).
[15] J. L. F. Da Silva, C. Stampfl, and M. Scheffler, Phys. Rev. Lett. **90**, 066104 (2003).
[16] G. Kresse and J. Furthmüller, Comput. Mater. Sci. **6**, 15 (1996).
[17] P. E. Blöchl, Phys. Rev. B **50**, 17 953 (1994).
[18] J. P. Perdew, K. Burke, and M. Ernzerhof, Phys. Rev. Lett. **77**, 3865 (1996).
[19] M. Petersen, S. Wilke, P. Ruggerone, B. Kohler, and M. Scheffler, Phys. Rev. Lett. **76**, 995 (1996).
[20] J. L. F. Da Silva and C. Stampfl, Phys. Rev. B **77**, 045401 (2008).
[21] P. Lazić, Ž. Crljen, R. Brako, and B. Gumhalter, Phys. Rev. B **72**, 245407 (2005).
[22] M. Rohlfing and T. Bredow, Phys. Rev. Lett. **101**, 266106 (2008).
[23] G. Román-Pérez and J. M. Soler, Phys. Rev. Lett. **103**, 096102 (2009).
[24] M. Dion, H. Rydberg, E. Schröder, D. C. Langreth, and B. I. Lundqvist, Phys. Rev. Lett. **92**, 246401 (2004); **95**, 109902(E) (2005); D. C. Langreth *et al.*, J. Phys. Condens. Matter **21**, 084 203 (2009).
[25] J. Klimeš, D. Bowler, and A. Michaelides, Phys. Rev. B **83**, 195131 (2011).
[26] N. Ferralis, H. I. Li, K. J. Hanna, J. Stevens, H. Shin, F. M. Pan, and R. D. Diehl, J. Phys. Condens. Matter **19**, 056 011 (2007).
[27] M. Pierno, L. Bruschi, G. Fois, G. Mistura, C. Boragno, F. Buatier de Mongeot, and U. Valbusa, Phys. Rev. Lett. **105**, 016102 (2010).